Non-invasive imaging prediction of tumor hypoxia

Radiotherapy and Oncology 153 (2020) 97–105

Contents lists available at ScienceDirect

Radiotherapy and Oncology

journal homepage: www.thegreenjournal.com

Original Article

Non-invasive imaging prediction of tumor hypoxia: A novel developed and externally validated CT and FDG-PET-based radiomic signatures

Sebastian Sanduleanu [a,*], Arthur Jochems [a], Taman Upadhaya [b,c], Aniek J.G. Even [a], Ralph T.H. Leijenaar [a], Frank J.W.M. Dankers [d], Remy Klaassen [f], Henry C. Woodruff [a,k], Mathieu Hatt [b], Hans J.A.M. Kaanders [d], Olga Hamming-Vrieze [e], Hanneke W.M. van Laarhoven [f], Rathan M. Subramiam [g,h], Shao Hui Huang [i], Brian O'Sullivan [i], Scott V. Bratman [i], Ludwig J. Dubois [j], Razvan L. Miclea [k], Dario Di Perri [l,m], Xavier Geets [l,m], Mireia Crispin-Ortuzar [n,o], Aditya Apte [n], Joseph O. Deasy [n], Jung Hun Oh [n], Nancy Y. Lee [p], John L. Humm [n], Heiko Schöder [q], Dirk De Ruysscher [r], Frank Hoebers [r], Philippe Lambin [a,k]

[a] The-D-Lab, Dpt of Precision Medicine, GROW - School for Oncology, Maastricht University Medical Centre+, The Netherlands; [b] Laboratory of Medical Information Processing (LaTIM), INSERM, UMR 1101, Univ Brest; [c] Department of Radiation Oncology, University of California, 1600 Divisadero Street, CA 94115, San Francisco, United States; [d] Department of Radiation Oncology, Radboud University Nijmegen Medical Centre; [e] Department of Radiation Oncology, Antoni van Leeuwenhoek - Netherlands Cancer institute, Amsterdam, The Netherlands; [f] Department of Medical Oncology, Cancer Center Amsterdam, Amsterdam UMC, University of Amsterdam, Amsterdam, The Netherlands; [g] Boston University School of Medicine; [h] Division of Nuclear Medicine, Russell H Morgan Department of Radiology and Radiologic Sciences, Johns Hopkins Medical Institutions, Baltimore, United States; [i] Department of Radiation Oncology, Princess Margaret Cancer Center, University of Toronto, Canada; [j] Department of Precision Medicine, The M-LAB, GROW - School for Oncology and Developmental Biology; [k] Department of Radiology and Nuclear Imaging, GROW - school for Oncology, Maastricht University Medical Centre+, The Netherlands; [l] Center of Molecular Imaging, Radiotherapy and Oncology (MIRO), Institut de Recherche Expérimentale et Clinique (IREC), Université catholique de Louvain; [m] Department of Radiation Oncology, Cliniques universitaires Saint-Luc, Brussels, Belgium; [n] Department of Medical Physics, Memorial Sloan Kettering Cancer Center, New York, United States; [o] Cancer Research UK Cambridge Institute, University of Cambridge, UK; [p] Department of Radiation Oncology, Memorial Sloan Kettering Cancer Center; [q] Department of Radiology, Memorial Sloan Kettering Cancer Center, New York, United States; [r] Department of Radiation Oncology (Maastro), GROW – School for Oncology and Developmental Biology, Maastricht University Medical Centre+, The Netherlands

ARTICLE INFO

Article history:
Received 2 July 2019
Received in revised form 9 October 2020
Accepted 12 October 2020
Available online 1 November 2020

Keywords:
Radiomics
Tumor hypoxia

ABSTRACT

Background: Tumor hypoxia increases resistance to radiotherapy and systemic therapy. Our aim was to develop and validate a disease-agnostic and disease-specific CT (+FDG-PET) based radiomics hypoxia classification signature.

Material and methods: A total of 808 patients with imaging data were included: $N = 100$ training/$N = 183$ external validation cases for a disease-agnostic CT hypoxia classification signature, $N = 76$ training/$N = 39$ validation cases for the H&N CT signature and $N = 62$ training/$N = 36$ validation cases for the Lung CT signature. The primary gross tumor volumes (GTV) were manually defined by experts on CT. In order to dichotomize between hypoxic/well-oxygenated tumors a threshold of 20% was used for the [^{18}F]-HX4-derived hypoxic fractions (HF). A random forest (RF)-based machine-learning classifier/regressor was trained to classify patients as hypoxia-positive/ negative based on radiomic features.

Results: A 11 feature "disease-agnostic CT model" reached AUC's of respectively 0.78 (95% confidence interval [CI], 0.62–0.94), 0.82 (95% CI, 0.67–0.96) and 0.78 (95% CI, 0.67–0.89) in three external validation datasets. A "disease-agnostic FDG-PET model" reached an AUC of 0.73 (0.95% CI, 0.49–0.97) in validation by combining 5 features. The highest "lung-specific CT model" reached an AUC of 0.80 (0.95% CI, 0.65–0.95) in validation with 4 CT features, while the "H&N-specific CT model" reached an AUC of 0.84 (0.95% CI, 0.64–1.00) in validation with 15 CT features. A tumor volume-alone model was unable to significantly classify patients as hypoxia-positive/ negative. A significant survival split ($P = 0.037$) was found between CT-classified hypoxia strata in an external H&N cohort (n = 517), while 117 significant hypoxia gene-CT signature feature associations were found in an external lung cohort (n = 80).

Conclusion: The disease-specific radiomics signatures perform better than the disease agnostic ones. By identifying hypoxic patients our signatures have the potential to enrich interventional hypoxia-targeting trials.

* Corresponding author at: The-D-Lab, Dpt of Precision Medicine, GROW - School for Oncology, Maastricht University Medical Centre+, Universiteitssingel 40, 6229 ER Maastricht, The Netherlands.
E-mail address: s.sanduleanu@maastrichtuniversity.nl (S. Sanduleanu).

https://doi.org/10.1016/j.radonc.2020.10.016
0167-8140/

Since the early 1930s, it has been established that solid tumors contain oxygen-deficient (hypoxic) areas. Cells in such areas may cause tumors to become resistant to radiotherapy and chemotherapy, increase tumor aggressiveness, angiogenesis, and metastatic spread, resulting in a poor prognosis [1–4].

Over the past decades various techniques [5] have been used to determine solid tumor oxygenation status, including hypoxia staining markers e.g. perfusion CT or 2-nitroimidazoles such as pimonidazole and noninvasive quantitative PET imaging (most commonly [^{18}F]-FMISO, [^{18}F]-HX4, [^{18}F]-FAZA as well as other 2-nitroimidazoles) [5–7]. In an effort to validate the heterogeneous uptake of [^{18}F]-HX4 at the regional tumor level, a preclinical study found that [^{18}F]-HX4 derived hypoxic fractions (HF) in tumors are strongly correlated with HF's assessed by the staining marker pimonidazole [8]. Furthermore, a causal inference was observed between the pretreatment tumor oxygenation status (HF's were altered by carbogen/nicotinamide exposure) measured by [^{18}F]-HX4 and the treatment efficacy with a hypoxia activated prodrug (HAP) TH302 that selectively kills hypoxic cells [9]. Hypoxia PET imaging is complex to implement in clinical practice since these PET-agents generally tend to generate smaller signal-to-background ratios compared to e.g. [^{18}F]-FDG [10,11] (and consequently lower target-background image contrast), imaging is labor intensive (instruction multiple bed positions and acquisitions at multiple time point), costly (chemical process to produce the radioligand is expensive), lacking of standard calibration procedures and inconvenient for the patient due to the time-consuming acquisition protocols.

Several HAP trials have failed to demonstrate efficacy in pivotal clinical trials (e.g. Tirapazamine, Evofosfamide), putatively due to the lack of patient selection with clearly defined high levels of hypoxia [12]. Another contributing factors might be the complex biology and spatiotemporal heterogeneity of the target (e.g. difficulties with extravascular transport to target cells, high variability in hypoxic compartments in relatively short periods of time) [12,13].

Computed Tomography (CT) and ^{18}F-FDG-PET imaging, by contrast, are both routinely used in clinical practice for cancer diagnosis and treatment planning. Radiomics is a quantitative image analysis methodology using data-characterization algorithms to derive imaging biomarkers [14–16].

This current study expands on previous initiatives [17] in hypothesizing that radiomic biomarkers from CT and FDG-PET imaging can be used to identify tumor with significant hypoxic regions, as established using HX4-PET, FMISO-PET and FAZA-PET. With these characteristics we believe that we could "enrich" trials testing hypoxia targeting drugs or window-of-opportunity trial populations using CT- and FDG-PET-based radiomics to identify and/or follow hypoxic tumors [18,19].

The aim of this study was to develop an agnostic (multiple tumor sites) and site specific HX4 derived CT and FDG-PET based radiomics hypoxia signature, validate this on an external datasets and assess the prognostic value of the signature and their association with previously validated hypoxia-response genes. We hypothesize that a combination of CT and FDG-PET-derived features could lead to a model with a higher performance compared to either modality alone.

Materials and methods

Patient selection

Patients from six academic medical centers and eight registered clinical trials were included in the analysis and are presented in Supplementary Appendix A and B, consisting of six [^{18}F]-HX4 datasets, one [^{18}F]-FAZA dataset, one [^{18}F]-FMISO and one based on the exogenous immunohistochemical marker pimonidazole (a 2-nitroimidazole derivate). IRB approval was obtained for this retrospective analysis and informed consent was given from all patients in the individual trials.

Image acquisition

All patients underwent pretreatment diagnostic CT/ planning [^{18}F]-FDG PET/CT. Pretreatment [^{18}F]-HX4 PET static images were acquired 2 and/or 4 h post injection (h.p.i.) [20]. When available, only the 4 h.p.i. images were used, since this time point is related to a plateau phase in tracer uptake that has been associated with optimal imaging properties [8,21]. In the Boston and UCLouvain dataset only 2 h p.i. images were available, and according to previous literature a tumor-to-background ratio (TBR) threshold of 1.2 was used instead of 1.4 [21]. Details regarding the acquisition parameters, protocol, and scanner types are presented in Supplementary appendix B, including an analysis of the SUV_{mean} in the background ROI as function of PET-tracer acquisition times for 10 random HX4-PET, FAZA-PET and FMISO-PET patients with head and neck squamous cell carcinoma.

Image segmentation, analysis and ground truth hypoxia

Primary gross tumor volumes (GTV) were manually defined on CT by experienced radiation oncologists and/or radiologists. [^{18}F]-FDG PET images were included only if they were performed within a week prior or after [^{18}F]-HX4 PET imaging, to mitigate for the temporal changes in tumor hypoxia. For the lung, and H&N cancer cases the clinical delineations defined on the planning [^{18}F]-FDG PET/CTs were transferred to the [^{18}F]-HX4 CT by means of rigid registration with Mirada software v 1.2.0.59 (Mirada Medical, Oxford, UK). Air and bone were filtered out using windowing presets and the delineations were manually adjusted to reflect small anatomical changes. For the esophageal and pancreatic cancer cases repeated scans of the same patient were rigidly co-registered to match the first scan using the mutual information metric, followed by a rigid registration. The corresponding PET images were subsequently registered using the resultant registration vectors. After registration, the tumor area in the esophagus or pancreas, and the aorta were drawn on the [^{18}F]-HX4 CT. Separately acquired diagnostic contrast enhanced CT images were used as reference for better tumor localization.

Cutoffs of 10%, 20% and 30% were used for hypoxic fractions (HF) to dichotomize between well-oxygenized and hypoxic tumors, in accordance with previous studies [22–25]. For the calcu-

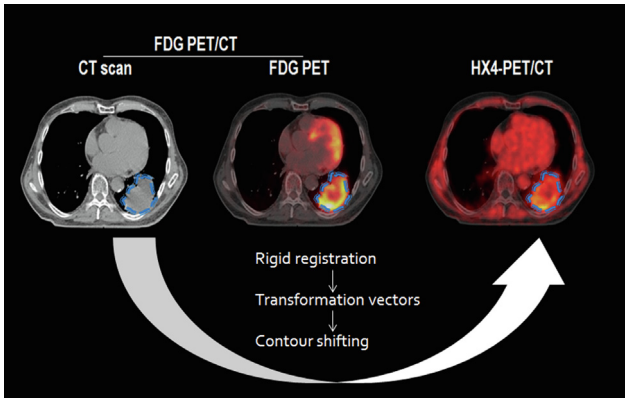

Fig. 1. Workflow resulting in [^{18}F]-HX4 and [^{18}F]- FDG-PET radiomic feature extraction and calculation of HF's on [^{18}F]-HX4. GTV delineations on diagnostic/baseline planning CT were rigidly registered onto the HX4-CT and contour transformation was performed from pre-treatment diagnostic/planning CT onto fused HX4 PET/CT.

lation of HF's, the following steps (See Fig. 1.) were followed in Reggui software v.1357 (OpenReggui, Louvain-la-Neuve, Belgium): (i) Contour GTV and aorta/muscle contour on HX4-CT. (ii) Resample and register HX4-PET to HX4-CT. (iii) Transfer GTV and aorta/-muscle contour to HX4-PET. (iv) Calculate average SUV_{aorta} and average SUV_{muscle} (dependent on tumor site). (v) On HX4-PET flag voxels as hypoxic (1) if SUV uptake per voxel/(mean aorta OR muscle uptake) $\geq$ 1.4 and non-hypoxic (0) if SUV uptake/(mean aorta OR muscle uptake) < 1.4. (vi) Calculate a HF as the number of hypoxic voxels/total number of VOI voxels. Additionally patients from a separate validation dataset (ARCON-trial) with fresh frozen biopsies obtained after 20-min i.v. infusion of 500 mg/m^2 of hypoxia marker Hypoxyprobe-1 (pimonidazole hydrochloride; NPI, Inc., Belmont, MA) were analyzed for association of the hypoxia radiomics signature with underlying histopathology [25]. For these cases the HF was defined as the tumor area positive for pimonidazole relative to the total tumor area in immunohistochemical analysis.

Image pre-processing and radiomic feature extraction/harmonization

International Biomarker Standardization Initiative (IBSI)-compliant radiomic features (https://ibsi.readthedocs.io/) as well as other non-IBSI covered features were extracted from both pre-treatment [^{18}F]-HX4-CT's as well as diagnostic [^{18}F]-FDG PET with our in-house RadiomiX research software (supported by Oncoradiomics, Liège, Belgium) implemented in Matlab 2017a (Mathworks, Natick, Mass). Computation of all features (including IBSI) is described in [26,27].

Houndsfield Unit (HU) intensities beyond −1024 and +3071 HU were clipped (assigned the value −1024 and +3071 respectively). An image intensity discretization with a fixed bin width of 25 Houndsfield Units (HU) and a standardized uptake value (SUV) of 0,50 was used for feature extraction in CT and FDG-PET respectively [28,29].

The algorithm used to convert polygonal-based segmentations to a voxel-based mask are described in [30]. The Fractal Dimension (FD) of the image is computed as described by Al-Kadi and Watson [31]. One-level and undecimated three dimensional wavelet transform was applied to each CT image (after resampling), which decomposes the original image X into 8 decompositions [26].

Voxel size resampling i.e., image interpolation was omitted for the agnostic model (See Table 1) in order to capture the full variability of the imaging data.

A total of 1222 CT and 1340 PET features were extracted from each image, consisting of five main groups: (1) fractal features (2) first order statistics, (3) shape and size, (4) texture descriptors including gray level co-occurrence (GLCM), gray level run-length (GLRLM) and gray level size-zone texture matrices (GLSZM), (5) features from groups 1, 3 and 4 after wavelet decomposition. There were no missing feature values. Definitions and detailed feature descriptions are described elsewhere [14].

Images from the site-specific models were resampled to a voxel size of $1 \times 1 \times 5$ mm^3 using cubic. This 'standard' voxel size was chosen according to the highest slice thickness and the median pixel spacing.

Radiomic feature values are potentially sensitive to inter-scanner model, acquisition protocol and reconstruction settings variation. The parametric ComBat statistical feature harmonization technique presented in Appendix F was employed in our analysis of radiomic features derived from CT. This technique was initially developed by Johnson et al. [32] for gene expression microarray data (even for small sample sizes) and was recently exploited in multicenter PET, MRI and CT radiomic studies [33,34].

Table 1
Model oversight section including name of model ($CT_{Agnostic}$, CT_{Lung}, etc…), datasets used in training and validation (including size and tumor site), percentage of patients that have a tumor with HF > 20%, hypoxia PET-tracer used to train and validate the models.

Models	Dataset training (n)	Imaging modality hypoxia (% hypoxic)	Trial registration number	Dataset validation (n)	Trial registration number	Imaging modality Hypoxia (% hypoxic)
$CT_{Agnostic}$	MAASTRO H&N (20) MAASTRO Lung Nitro (30) MAASTRO Lung PET boost (24) AMC EC & PC (26)	HX4 (22) HX4 (27) HX4 (17) HX4 (44)	NCT01347281 NCT01210378 NCT01024829 NCT01989000	1. Nijmegen ARCON H&N (40) 2. NKI/Boston Lung/ H&N (31) 3. UCL Lung (36) 4. MSKCC H&N (76)	NCT00147732 NCT01504815 and NCT01075399 Not yet registered NTC00606294	Only pimonidazole (0) HX4 (48) FAZA (36) FMISO (25)
$FDG_{Agnostic}$	MAASTRO Lung Nitro (21) MAASTRO Lung PET boost (6) MAASTRO H&N (5)	HX4 (19) HX4 (17) HX4 (22)	NCT01210378 NCT01024829 NCT01347281	MAASTRO Lung PET boost (15) MAASTRO H&N (9) Boston Lung (6)	NCT01024829 NCT01347281 NCT01075399	HX4 (17) HX4 (22) HX4 (40)
$CT_{Agnostic,(Combat),}$ SMOTE	Same as $CT_{Agnostic}$ (139 with Combat + SMOTE, 148 with SMOTE alone)	HX4 (51)	NCT01347281 NCT01210378 NCT01024829 NCT01989000	1. Nijmegen ARCON H&N (40) 2. NKI/Boston Lung/ H&N (31) 3. UCL Lung (36) 4. MSKCC H&N (76)	NCT00147732 NCT01504815 and NCT01075399 Not yet registered NTC00606294	Only pimonidazole (0) HX4 (48) FAZA (36) FMISO (25)
$FDG_{Agnostic,\ (Combat),}$ SMOTE	Same as $FDG_{Agnostic}$, (62 with Combat + SMOTE, 61 with SMOTE alone)	HX4 (51)	NCT01210378 NCT01024829 NCT01347281	MAASTRO Lung PET boost (15) MAASTRO H&N (9) Boston Lung (6)	NCT01024829 NCT01347281 NCT01075399	HX4 (17) HX4 (22) HX4 (40)
$(CT+FDG)_{Agnostic,}$ (Combat), SMOTE	Same as $CT_{Agnostic}$ and $FDG_{Agnostic}$ (61 with Combat +SMOTE, 64 with Combat alone)	HX4 (50)	NCT01024829 NCT01347281 NCT01075399	MAASTRO Lung PET boost (15) MAASTRO H&N (9) Boston Lung (6)	NCT01024829 NCT01347281 NCT01075399	HX4 (17) HX4 (22) HX4 (40)
$CT_{Lung,\ Combat}$	MAASTRO Lung Nitro (29) MAASTRO Lung PET boost (25) Boston Lung (8)	HX4 (24) HX4 (16) HX4 (50)	NCT01210378 NCT01024829 NCT01075399	UCL Lung (36)	Not yet registered	FAZA (36)
$CT_{Lung,\ Combat,\ SMOTE}$	Same as $CT_{Lung,\ combat}$ (98)	HX4 (52)	NCT01210378 NCT01024829 NCT01075399	UCL Lung (36)	Not yet registered	FAZA (36)
$CT_{H\&N,\ Combat}$	MSKCC H&N (76)	FMISO (25)	NTC00606294	Boston H&N (10) NKI H&N (12) MAASTRO H&N (17)	NCT01075399 NCT01504815 NCT01347281	HX4 (50) HX4 (50) HX4 (18)
$CT_{H\&N,\ Combat,\ SMOTE}$	Same as $CT_{H\&N,\ combat}$ (118)	FMISO (51)	NTC00606294	Boston H&N (10) NKI H&N (12) MAASTRO H&N (17)	NCT01075399 NCT01504815 NCT01347281	HX4 (50) HX4 (50) HX4 (18)

Statistical analysis

The statistical analysis for model development was performed with R studio software, version 3.3.4 downloadable from http://www.R-project.org. The R packages used in this study are described in Appendix G. Area under the curve (AUC), accuracy, positive and negative predictive value metrics were used to assess the performance of the models.

The independent samples Mann-Whitney test was used for comparison of unpaired, continuous data and the chi-square and Fisher's exact test was used for the comparison of categorical variables. All reported statistical significance levels were two-sided, with a significance level <0.05. Confidence intervals for accuracy were calculated with the confusionMatrix function in the Caret package v. 3.45. Confidence intervals for AUC were calculated with the ROC function in pROC. By default, this function uses 2000 bootstraps to calculate a 95% confidence interval. For reproducibility purposes, our source code can be found on the github repository: https://github.com/SebastianSanduleanu/RadiomicsHypoxiaSignature.git.

Machine learning model development

A random forest (RF) machine-learning classifier was computed (*default settings:* 500 trees, mtry = $\sqrt{\text{nr.of predictors}}$), with a 10-fold cross validation treebag recursive feature elimination algorithm (Caret package) loop reshuffled 10 times (outer resampling method whereby features were re-ranked) was used to classify patients as hypoxia-positive/negative based on the optimal combination of radiomic features. The final RF model was based on the nr. of features corresponding to the first peak in accuracy in the out of bag training cases. Regression trees were generated in order to treat the hypoxic fractions as a continuous variable.

Recursive feature elimination (RFE) is a feature selection method based on iterative model construction (e.g RF) to select features according to their performance (e.g classification error, importance) setting one subset of features aside and then repeating the process with the rest of the features, until all features in the dataset are exhausted. Features are then ranked according to when they were eliminated. As such, RFE is a greedy optimization procedure.

For both the CT and FDG-PET model a synthetic minority oversampling method (SMOTE) was used in R studio ('smotefamily' package, K = 5 nearest neighbors used for generating data) on the training dataset in order to achieve balanced classes. SMOTE is an oversampling technique that synthesizes a new minority instance (in feature space) between a minority instance and one of its K nearest neighbors [35]. The order in which the features were (pre-)processed were as following: Image resampling → Feature extraction → ComBat harmonization → SMOTE balancing → Recursive Feature Elimination → Random Forrest model with optimal amount of features.

In order to ascertain the feasibility of both agnostic (multiple solid tumor subsites such as esophagus, pancreas, lung and head and neck) as well as site-specific (lung and head and neck) hypoxia signatures we have generated the models represented in Fig. 2. Further details on the partitioning of the agnostic CT/ FDG-PET models are presented in Table 1.

Prognostic value and correlation with hypoxia-response genes

The CT's of 89 mainly early stage lung cancer patients acquired prior to surgery were downloaded from The Cancer Imaging Archive (TCIA) [14,36,37].

Primary GTV's were defined for n = 80 NSCLC patients, the rest (n = 9) was omitted due to lack of clear tumor boundaries on CT without availability of [^{18}F]-FDG PET.

Radiomic features were extracted from these images and agnostic $CT_{non\text{-}SMOTE}$ hypoxia signature outcome classes were generated according to the model splitting rules. Corresponding microarray data acquired for the imaging samples were available at National Center for Biotechnology Information (NCBI) Gene Expression Omnibus [38]. The results of this analysis are presented in Appendix E.

Clinical survival data was collected from yet another external head and neck cohort of n = 517 oropharyngeal head and neck squamous cell carcinoma patients from the Princess Margaret Cancer Centre in Toronto (details on this cohort are described in Fig. 3

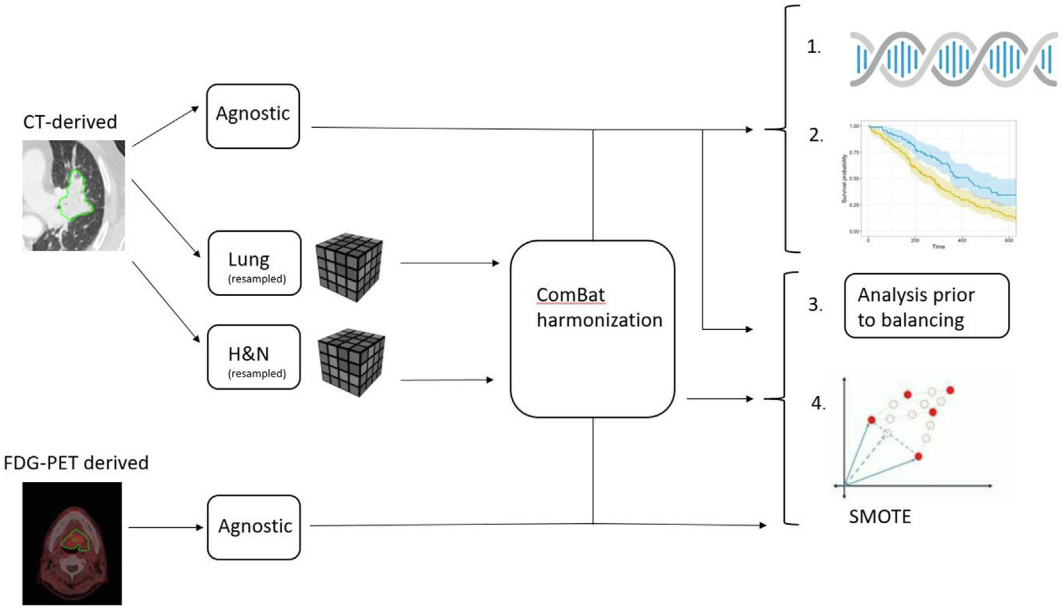

Fig. 2. Workflow of generated hypoxia-classification models. The agnostic classification signature was used to assess the association with the most relevant literature-derived hypoxia-response genes (1) and the prognostic value on an independent validation cohort (2). All generated signature performances were assessed prior to and after SMOTE (3–4). Site-specific (H&N, Lung) CT images were resampled to 1 × 1 × 5 mm^3 and radiomic feature values were harmonized, while agnostic features were directly analyzed before and after balancing the outcome classes.

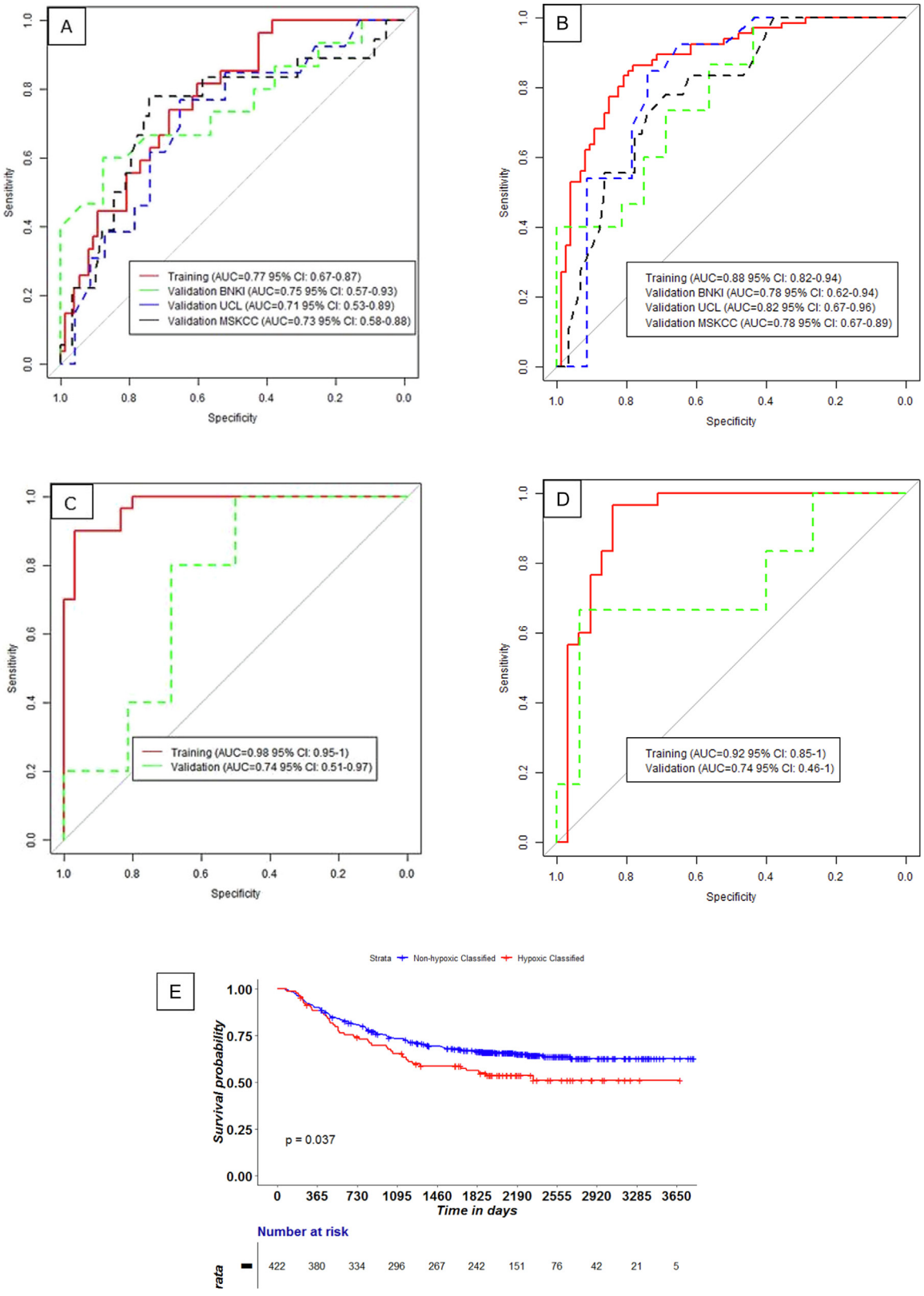

Fig. 3. (a) Training and validation AUC's presented for HF cutoff of 20% in agnostic CT model. (b). Training and validation AUC presented for HF 20% cutoff in agnostic CT $_{\text{ComBat, SMOTE}}$ model. (c) Training and validation AUC presented for HF 20% cutoff in agnostic FDG-PET$_{\text{SMOTE}}$ model. (d) Training and validation AUC presented for HF 20% cutoff in agnostic (CT + FDG-PET$_{\text{ComBat, SMOTE}}$ model. (e) Kaplan-Meier survival curves for overall survival (OS) according to the CT$_{\text{Agnostic, non-SMOTE}}$ hypoxia signature predicted classes on PMH head and neck cohort (n = 517).

and Appendix D). Radiomic features were subsequently extracted from these images and agnostic $CT_{non\text{-}SMOTE}$ hypoxia signature outcome classes were generated according to the model splitting rules.

Radiomics quality assurance and TRIPOD statement

For additional quality assurance a radiomics quality score (RQS) was calculated [39].

Scores were likewise calculated for the 22-item adherence data extraction TRIPOD (Transparent reporting of a multivariable prediction model for individual prognosis or diagnosis) 3 checklist.

Results

A total of 808 patients with imaging data were included, from which 221 patients with ground-truth hypoxia-PET: 131 patients with [^{18}F]-HX4 PET, 14 patients with up to three [^{18}F]-FAZA imaging timepoints (n = 36) and 76 patients with [^{18}F]-FMISO-PET. From this total group 61 patients had available FDG-PET images acquired within a week of hypoxia-PET. One lesion was delineated per patient. In total n = 100 training cases were available for the disease-agnostic CT hypoxia classification signature and n = 183 testing cases from 4 different independent validation cohorts. A total of n = 40 training cases and n = 21 external validation cases were available for the disease agnostic FDG-PET signature. A total of n = 76 training cases and n = 39 external validation cases were available for the H&N CT signature, while a total of n = 62 training cases and n = 36 validation cases were available for the Lung CT signature. See Supplementary Appendix C and Table 1 for an elaborate presentation of all model performances and for reflection of underlying class distributions.

The agnostic $CT_{non\text{-}SMOTE,\ non\text{-}Combat}$ RF model reached an AUC of 0.77 (0.95% confidence interval [CI], 0.67–0.87) in the CT training set (n = 100) with a 10-fold cross validation loop reshuffled 10 times, an AUC of 0.75 (0.95% CI, 0.57–0.93) in the Boston/NKI validation dataset (n = 31), an AUC of 0.73 (0.95% CI, 0.58–0.88) on the MSKCC and an AUC of 0.71 (0.95% CI, 0.53–0.89) in the UCLouvain validation set (n = 36) by combining 12 CT-derived radiomic features to classify hypoxia according to a HF cutoff of 20% (Table 2). Accuracy in the Boston/NKI validation dataset was 74%, 64% in the MSKCC dataset and 63% in the UCLouvain validation set, with positive and negative predictive values (PPV, NPV) of 70% and 82% for Boston/ NKI, 65% and 50% for UCLouvain and 89 and 37% for MSKCC respectively.

After batch normalization and synthetic minority class oversampling a CT model reached an AUC of 0.88 (0.95% CI, 0.94–0.82) in the training set (n = 139) with 10-fold cross validation loop reshuffled 10 times, an AUC of 0.78 (0.95% CI, 0.62–0.94) in the Boston/NKI, 0.82 (0.95% CI, 0.67–0.96) in the UCL validation set and 0.78 (0.95% CI, 0.67–0.89) in the MSKCC dataset respectively by combining 11 CT-derived radiomic features to classify hypoxia according to a hypoxic fraction cutoff of 20% (Table 2). A tumor volume-alone model was unable to significantly classify patients as hypoxia-positive/ negative with an AUC of 0.69 (0.95% CI, 0.49 to 0.89) in the Boston/ NKI, 0.52 (0.95% CI, 0.32 to 0.71) in the UCL validation set and 0.49 (0.95% CI, 0.33 to 0.65) in the MSKCC dataset respectively.

Accuracy in the UCL validation dataset (n = 36) was 64%, 52% for the Boston/NKI validation dataset (n = 31) and 76% for the MSKCC dataset (n = 76) with the $CT_{ComBat,\ SMOTE}$ model, with positive and negative predictive values of 63%, 52%, 76% and 100%, 100%, 100% respectively.

For the lung-specific $CT_{non\text{-}SMOTE,\ ComBat}$ signature the agnostic RF model reached an AUC of 0.75 (0.95% CI, 0.61–0.89) in training (n = 62, Boston, MASTRO nitro/PET-boost) and an AUC of 0.80 (0.95% CI, 0.65–0.95) in the validation set (UCL) by combining 4 CT-derived radiomic features (HF cutoff 20%, Table 2).

For the H&N-specific $CT_{non\text{-}SMOTE,\ ComBat}$ signature the agnostic RF model reached an AUC of 0.76 (0.95% CI, 0.63–0.89) in training (n = 76, MSKCC) and an AUC of 0.86 (0.95% CI, 0.66–1.00) in the validation set (Maastro, NKI) by combining 6 CT-derived radiomic features (HF cutoff 20%, Table 2).

A significant survival split (P = 0.037) was found between CT-classified hypoxia strata in an external H&N cohort (n = 517), while 117 low, but significant hypoxia gene-CT signature feature associations were found in an external lung cohort (n = 80).

For initial quality assurance of the radiomics workflow the outcomes of the entire CT cohort was randomized. Training a $CT_{non\text{-}SMOTE}$-model on the randomized outcomes resulted in an AUC of 0.59 (0.95% CI, 0.40–0.78) in external validation. The radiomics quality score (RQS) was calculated [39]. This resulted in a score of 67%. Most points were allocated for prospective trial inclusion (7 points), the use of 3 external validation datasets (5 points) and the use of feature reduction analysis (3 points). Scores were likewise calculated for the 22-item adherence data extraction checklist of the TRIPOD (Transparent reporting of a multivariable prediction

Table 2
Summary of disease-agnostic and disease-specific model performance parameters according to HF20% threshold. 1. Boston-NKI 2. UCLouvain 3. MSKCC.

Model	Patients training	Number features in model	AUC external validation	Confidence Interval	Accuracy testing	95% Confidence Interval	PPV (%)	NPV (%)
$CT_{Agnostic}$	100	12	1. 0.75 2. 0.71 3. 0.73	1. [0.57, 0.93] 2. [0.53, 0.89] 3. [0.58, 0.88]	1. 0.74 2. 0.64 3. 0.63	1. [0.55, 0.88] 2. [0.46, 0.79] 3. [0.51, 0.74]	1.70 2.65 3.89	1.82 2.50 3.37
$CT_{Agnostic,\ SMOTE}$	148	5	1. 0.79 2. 0.76 3. 0.72	1. [0.63, 0.95] 2. [0.58, 0.94] 3. [0.58, 0.87]	1. 0.61 2. 0.69 3. 0.51	1. [0.42, 0.78] 2. [0.52, 0.84] 3. [0.40, 0.63]	1. 70 2. 75 3. 92	1. 57 2. 58 3. 31
$CT_{Agnostic,\ Combat,\ SMOTE}$	139	11	1. 0.78 2. 0.82 3. 0.78	1. [0.62, 0.94] 2. [0.67, 0.96] 3. [0.67, 0.89]	1. 0.52 2. 0.64 3. 0.76	1. [0.33, 0.70] 2. [0.46, 0.79] 3. [0.65, 0.85]	1. 52 2. 63 3. 76	1. 100 2. 100 3. 100
$(CT + FDG)_{Agnostic,\ SMOTE}$	64	9	0.86	[0.68, 1.0]	0.67	[0.43, 0.85]	90.0	45.5
$(CT + FDG)_{Agnostic,\ ComBat,\ SMOTE}$	61	9	0.74	[0.46, 1.0]	0.71	[0.48, 0.89]	84.6	50.0
$CT_{Lung,\ Combat,\ SMOTE}$	98	3	0.76	[0.59, 0.92]	0.72	[0.54, 0.86]	81	60
$CT_{H\&N,\ Combat,\ SMOTE}$	118	15	0.84	[0.64, 1.00]	0.76	[0.56, 0.90]	88	58
GTV_{prim} volume	100	1	1. 0.69 2. 0.52 3. 0.49	[0.49, 0.89] [0.32, 0.71] [0.33, 0.65]	1. 0.58 2. 0.50 3. 0.70	1. [0.39, 0.75] 2. [0.33, 0.67] 3. [0.58, 0.80]	1. 56 2. 59 3. 76	1. 67 2. 14 3. 22

model for individual prognosis or diagnosis), which was in the ranged of 0.86–0.92 statement (See Supplementary Appendix H).

Discussion

This study explores the possibility of obtaining a validated radiomics signature consisting of CT and/or FDG-PET derived imaging features for the prediction of tumor oxygenation status from routine medical images. When applied to the external validation datasets, our models yielded significantly higher than random AUC's for Boston-NKI, UCL, FDG-PET and combined CT and FDG-PET models. Furthermore Kaplan-Meier analysis revealed a significant ($P < 0.05$) split in terms of overall survival (OS) between the hypoxic and non-hypoxic CT-classified strata in an external HNSCC cohort. There were a total of 117 significant correlations between hypoxia response gene-radiomic features from the $CT_{Agnostic,\ non\text{-}SMOTE}$-signature after correction for multiple testing.

The relatively high positive predictive values in nearly all models in our opinion are a strong argument that the signature could be implemented as a usable tool for e.g. ultrahigh dose-rate (FLASH) radiotherapy (assuming that tumor hypoxia is needed to have obtain the differential FLASH effect), HAP-trial patient selection, which does not directly come out of the AUC's presented (still a lot of false positives and negatives).

To our knowledge this is the first study to train a radiomic signature that is able to predict solid tumor hypoxia derived from HF's inferred from [^{18}F]-HX4 imaging instead of a TBR_{max} threshold on one single voxel [15]. Another benefit over previous study was the use of robust feature reduction and advanced machine learning methods on a wide array of solid tumors, the use of separate external datasets, identification of high- and low probability of survival patient groups classified according to the hypoxia signature and the association between hypoxia imaging biomarkers and hypoxia-response genes.

We believe that although the agnostic CT radiomic signature only misclassified 3/40 patients on the ARCON dataset there is still some discrepancy between HX4 spatially derived (volumetric) information and single-section biopsy-derived pimonidazole immunohistochemical staining. In a pancreatic tumor study for instance, variance component analysis demonstrated greater inter- than intrapatient variability of hypoxia, and furthermore that multiple (4–5) tumor sections are required to provide a consistent evaluation of its extent in individual tumors [40].

Eventually the choice of cutoff thresholds (primarily HF 20%) was based on previous radiobiologic studies, e.g. Moulder and Rochwell et al. [22], which reviewed 92 HF determinations in 42 tumor systems. Most solid tumors, even those with diameters of 1–3 mm, exhibit according to this study HF's that may range from 10 to 30% [3]. In most experimental solid tumors, ~10–20% of the viable tumor cells are found to be sufficiently hypoxic to be fully radioresistant as measured by analyses of tumor cell survival, tumor growth, or tumor cure [23]. With regard to the wavelet features found in the various hypoxia classification models the following can be said.

Wavelet transforms are used to enhance different aspects of the image regarding spatial resolution. The features derived in e.g. the CT_{SMOTE} model were mainly texture and statistical-related (after wavelet decomposition in different but mostly lower frequency sub-bands, so different sharpening and smoothing filters had to be applied initially): in total three texture and two statistical features in the model.

The finding of highly ranked wavelet features could be attributed to the fact that non-enhanced CT images were used in the training and validation of the model, possibly introducing discrepancies in Poisson noise and image resolution [41,42].

An interesting finding is that of the multiple high total lesion glycolysis features (SUV_{mean} X metabolic tumor volume) [43] found in both FDG-PET and combined CT and FDG-PET models. We hypothesize that oxygen availability to cells decreases glucose oxidation, whereas oxygen shortage in hypoxic solid tumors consumes glucose faster in an attempt to produce ATP via the less efficient anaerobic glycolysis to lactate (Pasteur effect) [44].

Hypoxia-PET has been previously shown to provide reproducible and spatially stable results, significant spatial correlations with metabolic active tumor volumes on FDG-PET and prognostic value with regard to disease free survival and local tumor control [45–48]. Hence we believe we have identified a good ground truth measurement of hypoxia status for comparison to CT/ FDG-PET derived radiomics in the context of patient stratification for hypoxia-activated prodrug trials albeit with radiotherapy (e.g dose-escalation, dose-painting of hypoxic sub volumes) or systemic therapy (e.g hypoxic cytotoxic agents, immunotherapy)..

Other strengths of this study are the use of a robust feature selection and machine learning classifier in order to train and validate the eventual models. This training method has been extensively described in previous research, even in the context of radiomic studies and is highly reproducible [49–51]. Further strengths are the validation on multiple external cohorts and the assessment of hypoxia according to HF's.

Some limitations include: (i) The unbalanced data, which we have tried to account for by applying SMOTE analysis. (ii) In this cross-sectional study there is the concern that solid tumors are riddled with areas of mild-hypoxia leading to severe hypoxia and necrosis as well areas of acute hypoxia and re-oxygenation. The chaotic architecture of the tumor vasculature typically results in dynamic fluctuations in blood flow and therefore oxygen availability. These fluctuations result in distinctive patterns and represent a phenomenon described as 'cycling hypoxia', with frequencies that have been shown to vary between seconds to hours and even days [52]. (iii) Despite the fact that our main CT models are trained and validated using HX4-PET with similar acquisition times, the addition of other tracers and times decreases the accuracy and robustness of the study. (v) None of the datasets is complete in terms of availability of hypoxia PET + FDG-PET + CT and known survival outcomes.

With prospect to the future, the accurate quantification of hypoxia using PET requires modelling of—and correcting for—tracer properties, notably, the tracer distribution volume V_d [53,54]. Currently, such modelling requires a long dynamic PET imaging protocol, which places a greater burden on patients and machine workload, further impeding the uptake of hypoxia-PET imaging into clinical practice. Hence, there is a pressing need to develop simplified cost-efficient imaging biomarkers that correct for inter-patient PET imaging agent transport variances.

Future research should in our view focus on the accrual of larger amounts of patients in disease-specific hypoxia-PET trials, further improving acquisition timing and signal stability in hypoxia PET scanning protocols, correlating hypoxia PET-radiomics with 3D tumor histology, associating robust gene expression signatures with hypoxia radiomic signatures and training and validating models on higher volumes of data using the distributed learning approach [55–58].

In summary, our results indicate that a CT and [^{18}F] FDG-PET derived radiomic signature can both accurately classify tumor hypoxia according to literature-derived HF cutoffs. These findings further reinforce the assumption that we can "enrich" interventional trials with hypoxia-targeting agents and FLASH by identifying patients with tumors likely to be hypoxic. After validation on multi-institutional cohorts such a marker could be potentially useful for patient stratification in trials and situations where [^{18}F]-HX4 is not readily available.

Acknowledgements

Authors acknowledge financial support from ERC advanced grant (ERC-ADG-2015, n° 694812 - Hypoximmuno), ERC-PoC n°SEP-210494895, ERC-2020-PoC: 957565-AUTO.DISTINCT, Authors also acknowledge financial support from SME Phase 2 (RAIL - n °673780), EUROSTARS (DART, DECIDE, COMPACT-12053), the European Program H2020-2015-17 (ImmunoSABR - n° 733008, PREDICT - ITN - n° 766276, FETOPEN- SCANnTREAT - n° 899549, CHAIMELEON - n° 952172, EuCanImage – n° 952103), TRANSCAN Joint Transnational Call 2016 (JTC2016 "CLEARLY"- n° UM 2017-8295) and Interreg V-A Euregio Meuse-Rhine ("Euradiomics" - n° EMR4). This research is also supported by the Dutch technology Foundation STW/NWO (grant n° 10696 DuCAT & n° P14-19 Radiomics STRaTegy), which is the applied science division of NWO, and the Technology Programme of the Ministry of Economic Affairs.

Conflict of interest disclosure

Dr Philippe Lambin reports, within and outside the submitted work, grants/sponsored research agreements from Varian medical, Oncoradiomics, ptTheragnostic/DNAmito, Health Innovation Ventures. He received an advisor/presenter fee and/or reimbursement of travel costs/external grant writing fee and/or in kind manpower contribution from Oncoradiomics, BHV, Merck, Varian, Elekta, ptTheragnostic and Convert pharmaceuticals. Dr Lambin has shares in the company Oncoradiomics, Convert pharmaceuticals, MedC2 and LivingMed Biotech, he is co-inventor of two issued patents with royalties on radiomics (PCT/NL2014/050248, PCT/NL2014/050728) licensed to Oncoradiomics and one issue patent on mtDNA (PCT/EP2014/059089) licensed to ptTheragnostic/DNAmito, three non-patented invention (softwares) licensed to ptTheragnostic/DNAmito, Oncoradiomics and Health Innovation Ventures and three non-issues, non licensed patents on Deep Learning-Radiomics and LSRT (N2024482, N2024889, N2024889). He confirms that none of the above entities or funding was involved in the preparation of this paper. Dr. Woodruff and Dr. Jochems have (minority) shares in the company Oncoradiomics. Dr. Ralph Leijenaar has shares in, and is Chief Technology Officer of, the company Oncoradiomics. He is co-inventor of an issued patent with royalties related to radiomics (PCT/NL2014/050728) licensed to Oncoradiomics. No further foreseen conflicts of interest.

Appendix A. Supplementary data

Supplementary data to this article can be found online at https://doi.org/10.1016/j.radonc.2020.10.016.

References

[1] Muz B et al. The role of hypoxia in cancer progression, angiogenesis, metastasis, and resistance to therapy. Hypoxia (Auckl) 2015;3:83–92.
[2] Overgaard J. Hypoxic radiosensitization: adored and ignored. J Clin Oncol 2007;25:4066–74.
[3] Yao K et al. In vitro hypoxia-conditioned colon cancer cell lines derived from HCT116 and HT29 exhibit altered apoptosis susceptibility and a more angiogenic profile in vivo. Br J Cancer 2005;93:1356–63.
[4] Dewhirst MW et al. Cycling hypoxia and free radicals regulate angiogenesis and radiotherapy response. Nat Rev Cancer 2008;8:425–37.
[5] Challapalli A et al. Molecular mechanisms of hypoxia in cancer. Clin Transl Imaging 2017;5:225–53.
[6] Zegers CM, et al. Hypoxia imaging with [(1)(8)F]HX4 PET in NSCLC patients: defining optimal imaging parameters. Radiother Oncol 2013; 109: 58-64.
[7] Xu Z et al. (18)F-Fluormisonidazole in tumor hypoxia imaging. Oncotarget 2017;8:94969–79.
[8] Dubois LJ et al. Preclinical evaluation and validation of [18F]HX4, a promising hypoxia marker for PET imaging. PNAS 2011;108:14620–5.
[9] Peeters SG et al. TH-302 in combination with radiotherapy enhances the therapeutic outcome and is associated with pretreatment [18F]HX4 hypoxia PET imaging. Clin Cancer Res 2015;21:2984–92.
[10] Wack LJ et al. Comparison of [18F]-FMISO, [18F]-FAZA and [18F]-HX4 for PET imaging of hypoxia–a simulation study. Acta Oncol 2015;54:1370–7.
[11] Thorwarth D, Wack L-J, Mönnich D, et al. Hypoxia PET imaging techniques: data acquisition and analysis. Clin Transl Imaging 2017;5:489–96.
[12] Spiegelberg L et al. Hypoxia-activated prodrugs and (lack of) clinical progress: The need for hypoxia-based biomarker patient selection in phase III clinical trials. Clin Transl Radiat Oncol 2019;15:62–9.
[13] Mistry IN et al. Clinical advances of hypoxia-activated prodrugs in combination with radiation therapy. Int J Radiat Oncol Biol Phys 2017;98:1183–96.
[14] Aerts HJ et al. Decoding tumour phenotype by noninvasive imaging using a quantitative radiomics approach. Nat Commun 2014;5:4006.
[15] Lambin P, Rios-Velazquez E, Leijenaar R, et al. Radiomics: Extracting more information from medical images using advanced feature analysis. Eur J Cancer 2012;48:441–6.
[16] Lambin P, van Stiphout RGPM, Starmans MHW, et al. Predicting outcomes in radiation oncology-multifactorial decision support systems. Nat Rev Clin Oncol 2013;10:27–40.
[17] Crispin-Ortuzar M, Aditya Apte, Milan Grkovski, et al. Predicting hypoxia status using a combination of contrast-enhanced computed tomography and [18F]-Fluorodeoxyglucose positron emission tomography radiomics features. Radiother Oncol 2018;127:36–42.
[18] Spiegelberg L, Houben R, Niemans R, et al. Hypoxia-activated prodrugs and (lack of) clinical progress: The need for hypoxia-based biomarker patient selection in phase III clinical trials. Clin Transl Radiat Oncol 2019;15:62–9.
[19] Larue RTHM, Van de Voorde L, Berbee M, et al. A phase 1 'window-of-opportunity' trial testing evofosfamide (TH-302), a tumour-selective hypoxia-activated cytotoxic prodrug, with preoperative chemoradiotherapy in oesophageal adenocarcinoma patients. BMC Cancer 2016;16.
[20] Sanduleanu S, Wiel A, Lieverse RIY, Marcus D, Ibrahim A, Primakov S, et al. Hypoxia PET imaging with [18F]-HX4-A promising next-generation tracer. Cancers (Basel) 2020;12.
[21] Zegers CM, van Elmpt W, Wierts R et al. Hypoxia imaging with [18F]HX4 PET in NSCLC patients: defining optimal imaging parameters. Radiother Oncol, 2013; 109:58-64.
[22] Moulder JE, Rockwell S. Hypoxic fractions of solid tumors: experimental techniques, methods of analysis, and a survey of existing data. Int J Radiat Oncol Biol Phys 1984;10:695–712.
[23] Rockwell S et al. Hypoxia and radiation therapy: past history, ongoing research, and future promise. Curr Mol Med 2009;9:442–58.
[24] Brian DK, Robert DT. Stereotactic body radiation therapy. 2005; Lippincott Williams and Wilkins.
[25] Janssens GO et al. Accelerated radiotherapy with carbogen and nicotinamide for laryngeal cancer: results of a phase III randomized trial. J Clin Oncol 2012;30:1777–83.
[26] Peerlings J, Woodruff HC, Winfield,, et al. Stability of radiomics features in apparent diffusion coefficient maps from a multi-centre test-retest trial. Sci Rep 2019;9.
[27] Zwanenburg A et al. The image biomarker standardization initiative: standardized quantitative radiomics for high throughput image-based phenotyping. Radiology 2020;295:328–38.
[28] Leijenaar RT et al. The effect of SUV discretization in quantitative FDG-PET Radiomics: the need for standardized methodology in tumor texture analysis. Sci Rep 2015;5:11075.
[29] Larue R et al. Influence of gray level discretization on radiomic feature stability for different CT scanners, tube currents and slice thicknesses: a comprehensive phantom study. Acta Oncol 2017;56:1544–53.
[30] Mathworks website: https://www.mathworks.com/help/images/ref/poly2mask.html.
[31] Al-Kadi OS, Watson D. Texture analysis of aggressive and nonaggressive lung tumor CE CT images. IEEE Trans Biomed Eng 2008;55:1822–30.
[32] Johnson WE, et al. Adjusting batch effects in microarray expression data using empirical Bayes methods. Biostatistics 2007; 8: 118-127.
[33] Orlhac F et al. Validation of a method to compensate multicenter effects affecting CT radiomics. Radiology 2019;291:52–8.
[34] Lucia F et al. External validation of a combined PET and MRI radiomics model for prediction of recurrence in cervical cancer patients treated with chemoradiotherapy. Eur J NUCLouvain Med Mol Imaging 2019;46:864–77.
[35] Blagus R, Lusa L. SMOTE for high-dimensional class-imbalanced data. BMC Bioinformatics 2013;14:106.
[36] Aerts HJ et al. Data from NSCLC-radiomics-genomics. Cancer Imaging Arch 2015.
[37] Clark K et al. The Cancer Imaging Archive (TCIA): maintaining and operating a public information repository. J Digit Imaging 2013;26:1045–57.
[38] Gene Expression Omnibus (GEO) website: http://www.ncbi.nlm.nih.gov/geo/query/acc.cgi?acc=GSE58661.
[39] Lambin P, Leijenaar RT, Deist TM, et al. Radiomics: the bridge between medical imaging and personalized medicine. Nat Rev Clin Oncol 2017;14:749–62.
[40] Dhani NC, Serra S, Pintilie M, Schwock J, Xu J, Gallinger S, et al. Analysis of the intra- and intertumoral heterogeneity of hypoxia in pancreatic cancer patients receiving the nitroimidazole tracer pimonidazole. Br J Cancer 2015;113:864–71.
[41] Zhang B et al. Wavelets, ridgelets, and curvelets for Poisson noise removal. IEEE Trans Image Process 2008;17:1093–108.
[42] Borsdorf A et al. Wavelet based noise reduction in CT-images using correlation analysis. IEEE Trans Med ing 2008;27:1685–703.

[43] Larson SM et al. Tumor treatment response based on visual and quantitative changes in global tumor glycolysis using PET-FDG imaging. the visual response score and the change in total lesion glycolysis. Clin Positron Imaging 1999;2:159–71.
[44] Solaini G et al. Hypoxia and mitochondrial oxidative metabolism. Acta Biochim Biophys. 2010; 1797: 1171-1177.
[45] Rajendran JG, Krohn KA. F18 fluoromisonidazole for imaging tumor hypoxia: imaging the microenvironment for personalized cancer therapy. Semin NUCLouvain Med 2015;45:151–62.
[46] Mortensen LS et al. FAZA PET/CT hypoxia imaging in patients with squamous cell carcinoma of the head and neck treated with radiotherapy: results from the DAHANCA 24 trial. Radiother Oncol 2012;105:14–20.
[47] Zegers CML et al. Repeatability of hypoxia PET imaging using [F-18]HX4 in lung and head and neck cancer patients: a prospective multicenter trial. Eur J Nucl Med Mol Imaging 2015;42:1840–9.
[48] Zegers CM et al. In vivo quantification of hypoxic and metabolic status of NSCLC tumors using [18F]HX4 and [18F]FDG-PET/CT imaging. Clin Cancer Res 2014;20:6389–97.
[49] Parmar C et al. Machine learning methods for quantitative radiomic biomarkers. Sci Rep 2015;5:13087.
[50] Guyon I, Weston J, Barnhill S, Vapnik V. Gene selection for cancer classification using support vector machines. Mach Learn 2002;46:389–422.
[51] Kang Daesung, Park Ji Eun. Young-Hoon Kim et al., Diffusion radiomics as a diagnostic model for atypical manifestation of primary central nervous system lymphoma: development and multicenter external validation. Neuro-Oncology 2018:noy021.
[52] Eales KL et al. Hypoxia and metabolic adaptation of cancer cells. Oncogenesis 2016;5:e190.
[53] Taylor E et al. Impact of tissue transport on PET hypoxia quantification in pancreatic tumors. Ejnmmi Res 2017;7:101.
[54] Verwer EE, et al. Pharmacokinetic modeling of a novel hypoxia PET tracer [(18) F]HX4 in patients with non-small cell lung cancer. EJNMMI. Phys 2016; 3(1): 30.
[55] Deist TM et al. Machine learning algorithms for outcome prediction in (chemo) radiotherapy: An empirical comparison of classifiers. Med Phys 2018.
[56] Jochems A, et al. Developing and validating a survival prediction model for NSCLC patients through distributed learning across 3 countries. Int J Radiat Oncol Biol Phys. 2017; 99: 344-352. IF: 5.55
[57] Deist TM et al. Infrastructure and distributed learning methodology for privacy-preserving multi-centric rapid learning health care: euroCAT. Clin Transl Radiat Oncol 2017;4:24–31.
[58] Even AJG et al. Predicting tumor hypoxia in non-small cell lung cancer by combining CT, FDG PET and dynamic contrast-enhanced CT. Acta Oncol 2017;56:1591–6.
[59] Klaassen R et al. Feasibility and repeatability of PET with the hypoxia tracer [(18)F]HX4 in oesophageal and pancreatic cancer. Radiother Oncol 2015;116:94–9.
[60] Zegers CM et al. Imaging of tumour hypoxia and metabolism in patients with head and neck squamous cell carcinoma. Acta Oncol 2015;54:1378–84.
[61] Heukelom J et al. Adaptive and innovative Radiation Treatment FOR improving Cancer treatment outcomE (ARTFORCE); a randomized controlled phase II trial for individualized treatment of head and neck cancer. BMC Cancer 2013;13:84.
[62] Di Perri D et al. Evolution of [(18)F]fluorodeoxyglucose and [(18)F] fluoroazomycin arabinoside PET uptake distributions in lung tumours during radiation therapy. Acta Oncol 2017;56:516–24.
[63] Di Perri D et al. Correlation analysis of [(18)F]fluorodeoxyglucose and [(18)F] fluoroazomycin arabinoside uptake distributions in lung tumours during radiation therapy. Acta Oncol 2017;56:1181–8.
[64] Zhao Binsheng, Schwartz Lawrence H, Kris Mark G. Data from RIDER_Lung CT. The Cancer Imaging Archive; 2015.
[65] Zhao B, James LP, Moskowitz CS, Guo P, Ginsberg MS, Lefkowitz RA, et al. (2009, July). Evaluating variability in tumor measurements from same-day repeat CT scans of patients with non-small cell lung cancer 1. Radiology. Radiological Society of North America (RSNA).
[66] Clark K, Vendt B, Smith K, Freymann J, Kirby J, Koppel P, et al. The Cancer Imaging Archive (TCIA): maintaining and operating a public information repository. J Digit Imaging 2013;26:1045–57.
[67] Tawk B et al. Comparative analysis of transcriptomics based hypoxia signatures in head- and neck squamous cell carcinoma. Radiother Oncol 2016;118:350–8.
[68] Swinson DEB, O'Byrne KJ. Interactions between hypoxia and epidermal growth factor receptor in non-small-cell lung cancer. Clin Lung Cancer 2006;7:250–6.
[69] Ramachandran A et al. An in vivo hypoxia metagene identifies the novel hypoxia inducible factor target gene SLCO1B3. Eur J Cancer 2013;49:1741–51.
[70] Harris BHL et al. Gene expression signatures as biomarkers of tumour hypoxia. Clin Oncol 2015;27:547–60.
[71] Buffa FM, et al. Large meta-analysis of multiple cancers reveals a common, compact and highly prognostic hypoxia metagene. Br J Cancer. 2010; 103: 1136-1136.